4.2 Growth Model of Carbon Nanotubes by Using HWCVD

The reason for the growth of the CNTs is discussed here. Almost every previous report has indicated that the growth of the CNTs must be attributable to the catalytic effect, and the use of hydrocarbon as the carbon source. In this synthesis, alcohol was chosen as the carbon source for growing CNTs. In addition to CO_2, Ar gas was also used as a carrier gas in growing CNTs. However, Ar yields fewer CNTs than CO_2 does. Therefore, CO_2 may be a key component in enhancing the growth of CNTs, but the reason is not yet known. The fact that Ar can also be used suggests that no catalyst is present in the gas or vapor environment employed in this study; therefore, the Fe-Cr wire is the only possible catalyst source. The Fe-Cr wire consists of Fe (71.4 wt %), Cr (22.5 wt %) and others. In the present experiment, the temperature of the Fe-Cr wire is about 1200 ℃, which is lower than its melting point by 200~300 ℃. Under such conditions, the situation is similar to that of conventional vacuum evaporation coating, but with fewer evaporated atoms due to the lower temperature and absence of vacuum conditions. As shown in Fig. 18, the mixture of carrier gas and alcohol flows toward the Fe-Cr wire. In addition to this flow direction, other flow directions were also tested, but few and scattered CNTs formed on the substrate. Therefore, we consider that the evaporated metal atoms following the flow direction toward the silicon substrate will provide the catalyst for further growth of the CNTs.

CNTs were reported to be deposited as a by-product of diamond thick films in an HFCVD system [29]. That study suggested that the copper-covered parts near the hot filaments were evaporated *in situ* during deposition, mainly in the form of atomic clusters that might have enhanced catalysis due to the size effect. In this study, the wire used is not high-grade and has several impurities, being composed of Fe (71.4 %), Cr (22.5 %) and others. The surface stoichiometry of our nanotubes, characterized using AES, shows small amounts of Si (3.75 %), Al (4.89 %), O (3.33 %), Ni (4.99 %), Fe (6.37 %) and Cr (4.78 %) in the carbon (71.89 %). Figure 33 plots the profile of the wire and surface of the sample.
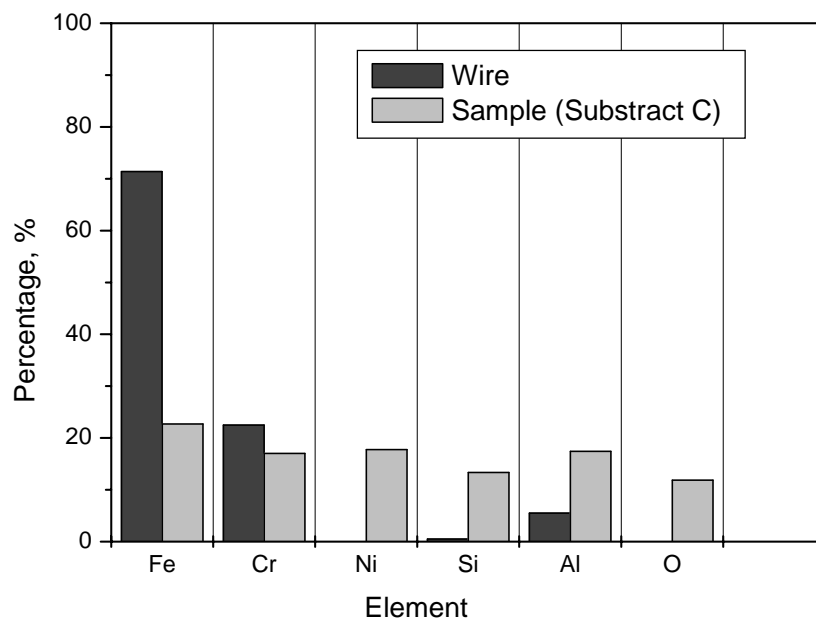
Fig. 33. Metal elements profile of the wire and surface of the sample.

Among the surface of CNTs, Si may arise due to the substrate effect, and Ni is the impurity associated with deposition at high temperature. Ni, Fe and Cr have been considered to act as catalysts in the synthesis of CNTs [28, 161-163]. Fe is the major element, at 6.37 at%, suggesting it plays a leading role in catalyzing the formation of these CNTs. In particular, Fe is considered the best catalyst for thermal CVD [164]. EDX attached to the TEM also shows that Fe atoms appear despite Fe particles disappear. On the other hand, we did not have sufficient experience using W wire for growing CNTs. The major reason is that W wire cannot stand a long time without fracture under the condition of using a mixture of CO_2 and alcohol. Indeed, we have confirmed that when using a mixture of H_2 and alcohol to deposit carbon, no CNTs were formed. This may be attributed to W having a much higher melting point (~2974 ℃). The metal particles should be supported on a substrate or introduced as 'floating' particles in a gas stream that flows through the reactor [165,166]. Therefore, we believe that *in situ* evaporated catalysts from the Fe-Cr wire should be used to grow CNTs.

We investigated TEM images to explain a growth mechanism of CNTs. Figure 34 shows TEM image of CNT consists of hollow compartments, similar to a bamboo-like structure. The TEM image reveals the closed tip without any encapsulated metal particles (see arrows 1) and the compartment layers whose curvature is directed toward the tip (see arrows 2). Figure 35(a) shows HRTEM image for the bamboo-like structure of CNT. The arrow 1 indicates the wall, and the arrow 2 indicates the compartment layers. There are some defective graphitic sheets at the surface of wall as indicated by arrow 3. Open roots separated from the metal particles are found, as shown in Fig. 35(b).

From HRTEM images, our CNTs comprise the following structural features: (i) There is no encapsulated metal particle at the closed tip and (ii) A bamboo-like structure with a compartment curvature directed to the tip. The bamboo structure has been found in the CNTs grown using arc discharge [167,168], microwave PECVD [120] and pyrolysis [169]. Therefore, it can be concluded that the formation of the bamboo structure should be possible regardless of the growth method used. However, the curvature of the compound layer in the bamboo-like CNTs grown using the above-mentioned PECVD and pyrolysis is directed to the root, which is opposite to that of our CNTs grown. Besides, those CNTs grown using PECVD or pyrolysis have an encapsulated catalytic particle at the tip, which is also different from our results. Thus, we suggest that the growth of CNTs follows a base-growth mechanism. Base-growth mechanism would be adequate to describe the closed tips that are free of encapsulated catalytic particles as well as the compartment curvature directed to the tip [170].
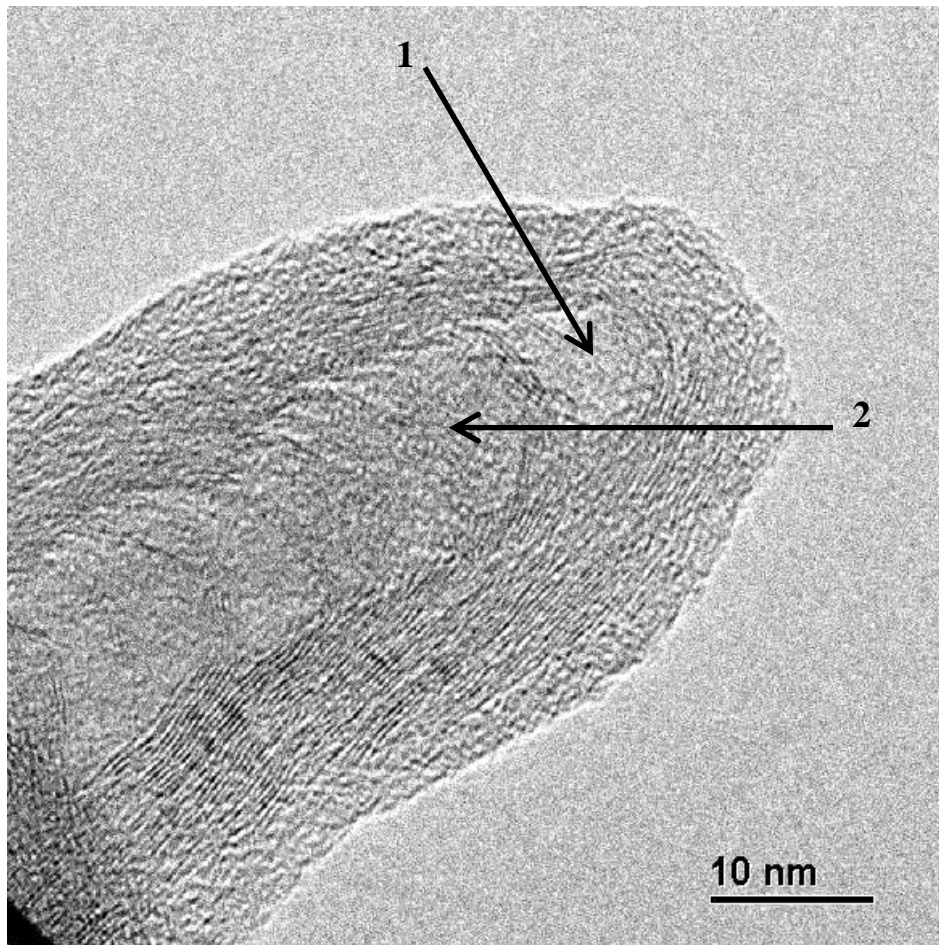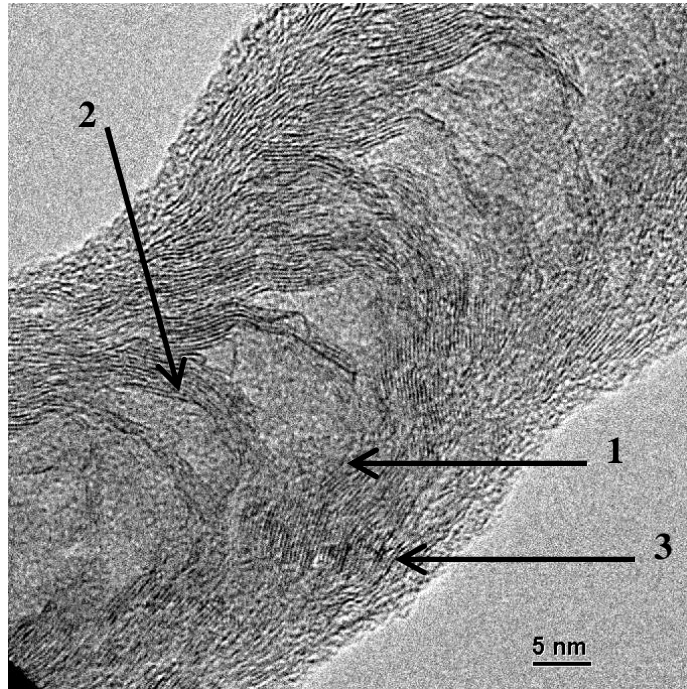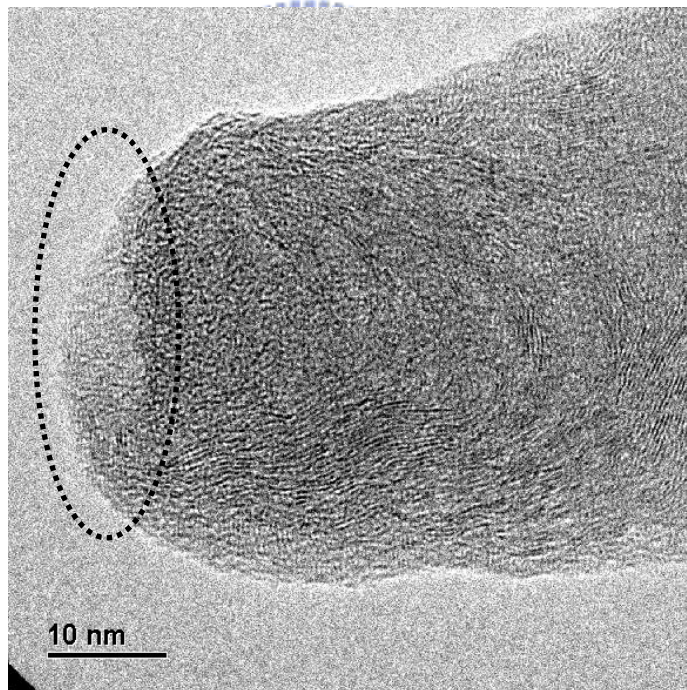
Fig. 34. TEM image of CNT grown exhibit a bamboo-like structure. The arrow 1 indicates the closed tips with no encapsulated metal particle. The arrow 2 corresponds to the compartment layers whose curvature is directed to the tip.

(a)

(b)

Fig. 35. (a) HRTEM image for the bamboo-like structure of CNT. The arrow 1 indicates the wall, the arrow 2 indicates the compartment layers, and the arrow 3 indicates defective graphitic sheets at the surface of wall. (b) Image indicates the open roots separated from catalyst particle.

The base-growth model was early developed for catalytic carbon filament growth by Baker et al [171]. They concluded that the filament can grow upward from the metal particles that remain attached to the substrate. Schematic diagrams of our whole growth model are shown in Fig. 36(a)-(e).

(a) Initially, metal atoms or clusters, which from the heating Fe-Cr wire, deposit on the substrate and start to coalesce. This process leads to the formation of catalytic particles.

(b) Carbons produced from the decomposition of alcohol adsorb on these catalytic particles. Then they diffuse via surface and bulk of metal particle to form the graphitic sheets as a cap on the catalytic particle.

(c) As the cap lifts off the catalytic particle, a closed tip with inside hollow is produced.

(d) The motive force departing from the catalytic particle may be the stress accumulated under the graphitic cap. The carbons accumulated at the inside surface of catalytic particle can form the compartment graphitic sheets [170]. The compartment layer will depart from the catalytic particle due to the stress.

(e) Once sufficient stress has been released the next wave of graphite layers can start to form the next compartment and the whole process is repeated. The irregular appearance of compartment layers with various thicknesses and shapes may be due to non-uniform carbon supply [170].

Accordingly; this method combines PVD and CVD to synthesize CNTs. In addition, since *in situ* evaporated catalysts from the filament were used to grow the CNTs, an alternating wire grid arrangement may support the scaling of the method, and continuous production may be attainable by *in situ* growth of CNTs which can be peeled off during the process.
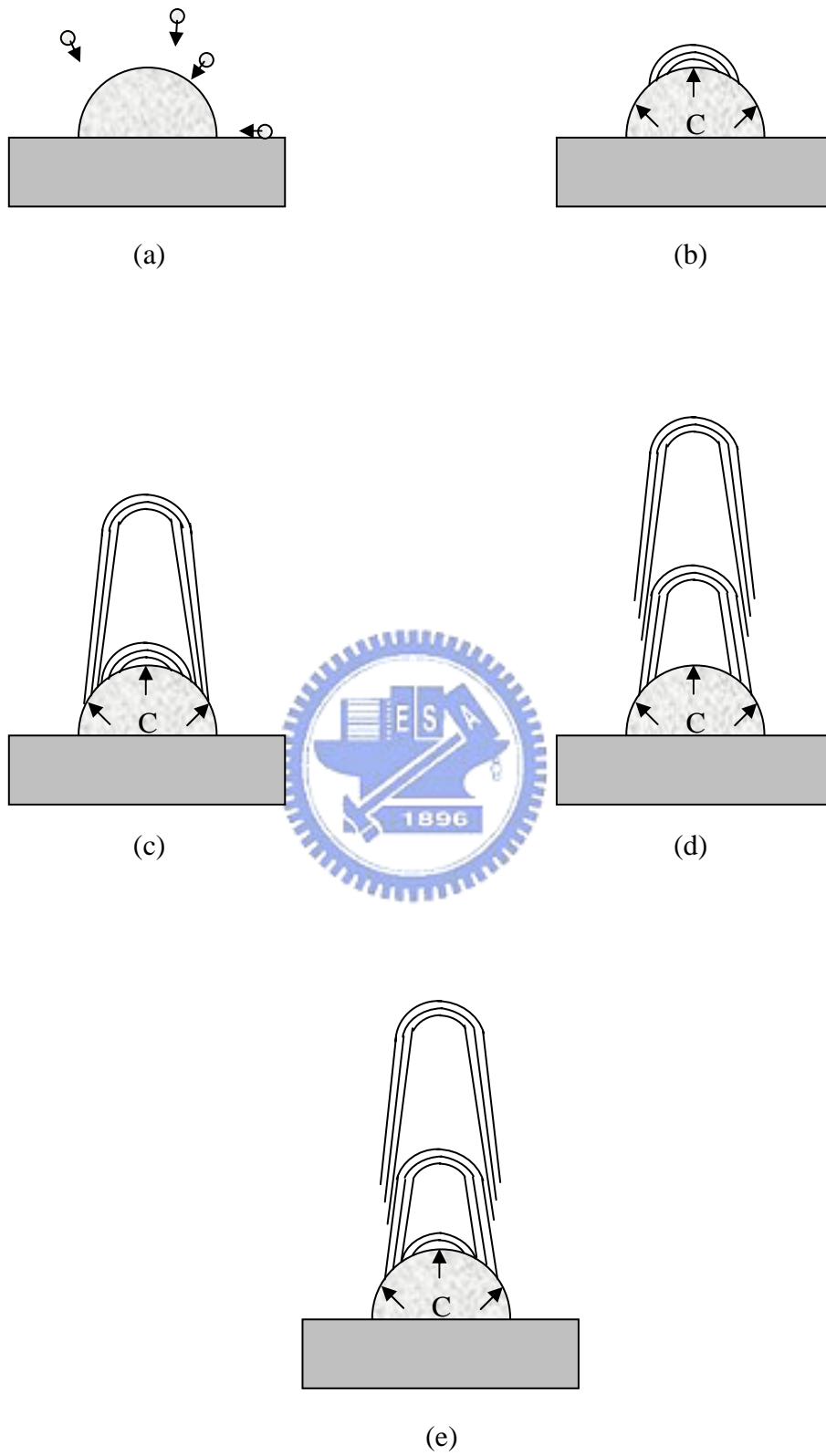
(a)

(b)

(c)

(d)

(e)

Fig. 36. Growth model of MWCNTs by using direct HWCVD

4.3 Carbon Nanotubes Grown on AISI 304 by Using MPCVD: CH_4/CO_2 Reactant Gas

Aligned carbon nanotubes were grown on stainless steel 304 by bias-enhanced microwave plasma chemical vapor deposition, using CH_4/CO_2 as the reactant gas. A bias was applied to the microwave plasma to grow the nanotubes over various periods. Experimental results show that well-aligned carbon nanotubes grow on stainless steel at a negative bias of -300 V. EDX on TEM indicated that the metal catalyst on the top of the carbon nanotubes includes Fe and Ni, but not Cr. The field emission properties of the resultant carbon nanotubes were obtained at a negative bias of -300 V: the emission current was 140 mA/cm^2 at 2 V/μm; and the turn-on field, which is the field needed to extract current density of 10 $\mu A/cm^2$, was 1.4 V/μm.

4.3.1 Background

It has been shown that CH_4/CO_2 can promote the growth rate over that obtained with CH_4/H_2, because of the high concentration of carbon [172]. The growth quality of CNTs has been reported to exceed that of obtained using a conventional reaction in a gas mixture of hydrogen and hydrocarbons [173], and the growth temperature can probably be reduced to under 300 °C [174].

In the authors' previous study, CNTs were grown *in situ* by modified hot filament chemical vapor deposition using an Fe-Cr wire (Fe: 71.4 wt %, Cr: 22.5 wt %) that acts as a catalyst and a heat source [175]. Furthermore, M. Okai et al. [28] reported the growth of carbon nanotubes on Fe-Ni-Cr alloy substrate (Fe: 52 wt %, Cr: 6 wt %, Ni: 42 wt %). Comparing, the alloy they used has much less Cr than that of our study. Therefore, in this work, typical stainless steel 304 (Fe: 70 wt %, Cr: 19 wt %, Ni: 9 wt %), an Fe-Ni-Cr alloy with a high Cr content, was used as the substrate to grow CNTs and identify the catalytic effects of the metal.

4.3.2 Effect of Bias on Growth of CNTs

By using MPCVD, the reactive gas mixture was CH_4/CO_2 at a flow rate of 30/22.5 sccm. The applied microwave power and pressure were 300 W and 1333 Pa, respectively. Figure 37 presents SEM photographs of deposition products grown for 10 min at various biases. The SEM photograph shown in Fig. 37(a) shows that CNTs grew on stainless steel 304 at a negative bias of -300 V. The surface morphology was almost the same across the entire area. Figure 37(b) shows that no CNTs grow on the stainless steel at no bias, and Fig. 37(c) shows that carbon rods grow on the stainless steel at a positive bias of +300 V. However, the morphologies of both samples differed between their corners and the center. Partial surface fragmentation has been reported [176] to produce a wide variety of surface structures, which then translates into a corresponding variety of catalyzed products, ranging from tufts, stumps, to CNTs.

Raman spectroscopy has been used to study MWCNTs [177]. The first-order Raman spectrum of the CNTs includes strong, sharp peaks at 1581 cm^{-1} and 1350 cm^{-1}, typical of graphitic carbon nanostructures. Figure 38 presents the Raman spectra of the deposition product grown on stainless steel 304 under various bias conditions for 10 min. As shown in Fig. 38, samples at biases of -300 V and +300 V yielded two peaks at around 1350 cm^{-1} and 1581 cm^{-1}. Furthermore, the Raman spectrum indicates that the sample grown under no bias yielded no carbon structure, as shown in Fig. 38(b).
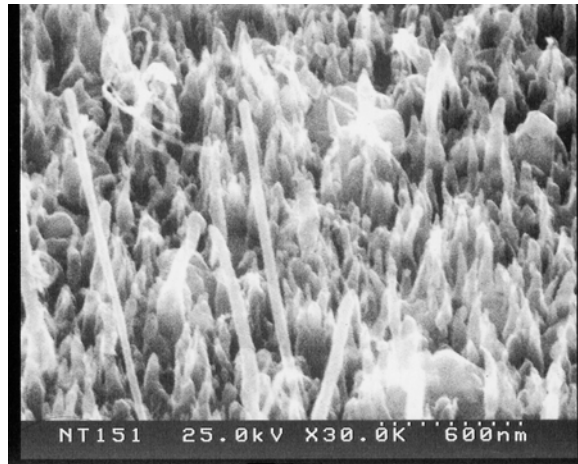
(a)
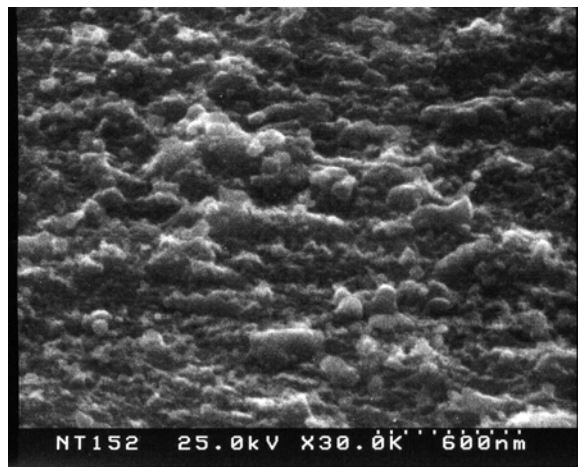
(b)
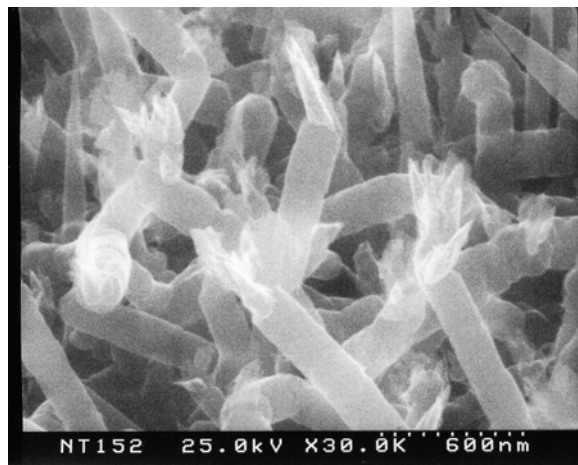
(c)

Fig. 37. SEM photographs of deposition product grown on stainless steel 304 at various biases for 10 min; (a) -300 V, (b) 0 V, and (c) +300 V.
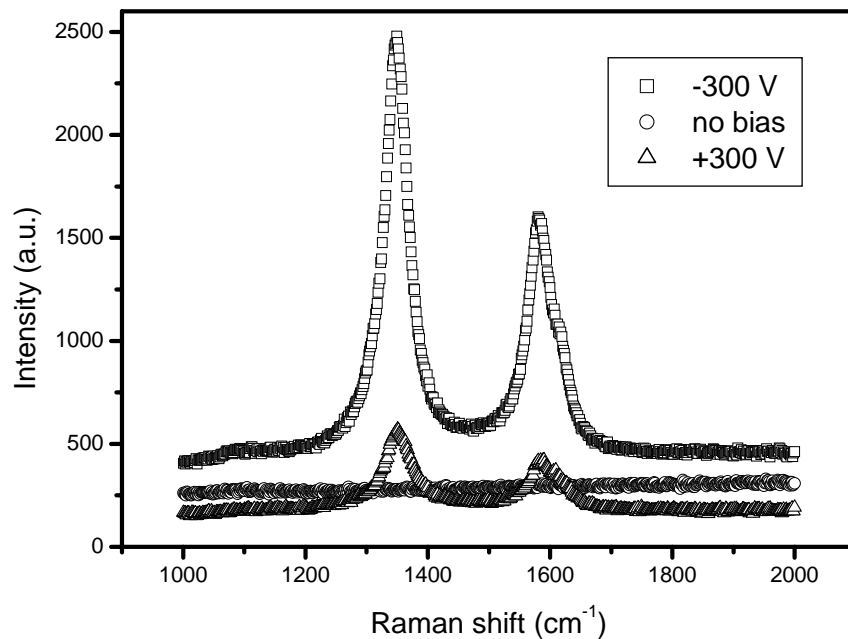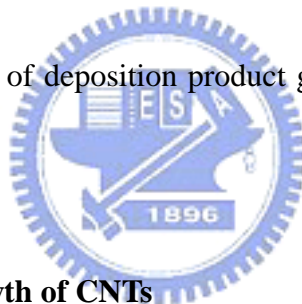
Fig. 38. Micro-Raman spectra of deposition product grown on stainless steel 304 at various biases for 10 min.

4.3.3 Various Periods of Growth of CNTs

From the SEM photographs and Raman spectra, a negative bias of -300 V was selected to examine the various periods of growth of CNTs. Figure 39 presents SEM photographs of CNTs grown on stainless 304 at a negative bias of -300 V for various periods. Figure 39(a) shows the surface breakup of stainless steel 304. The rupture of the surface has been reported [176] to have increased the yield of CNTs and the uniformity of their sizes. According to Figs. 39(a)-(d), the yield and diameter of CNTs increased with the growth time. Besides, vertical CNTs become more prevalent as growth time increases. As shown in Fig. 39(d), CNTs grown for 30 min possess a high-aspect-ratio, implying potential use as field emission devices.
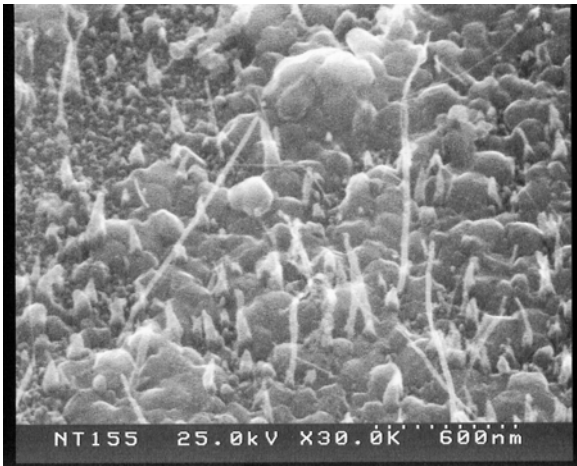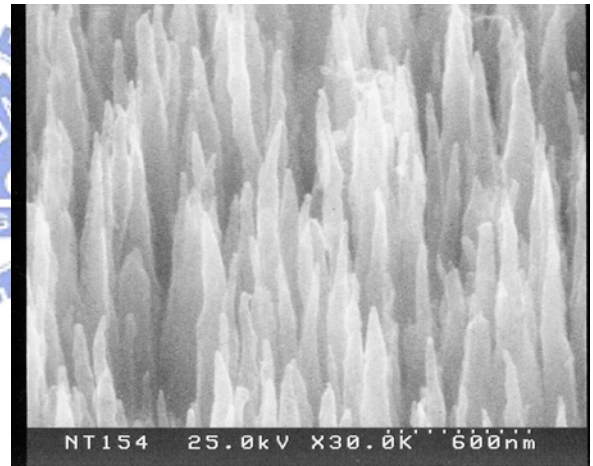
(a) 5 min
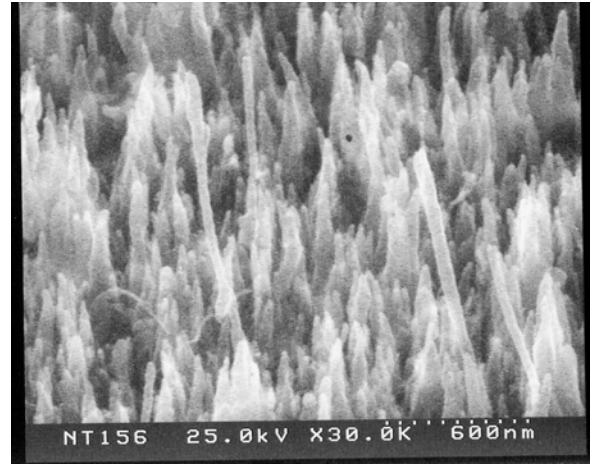
(c) 15 min
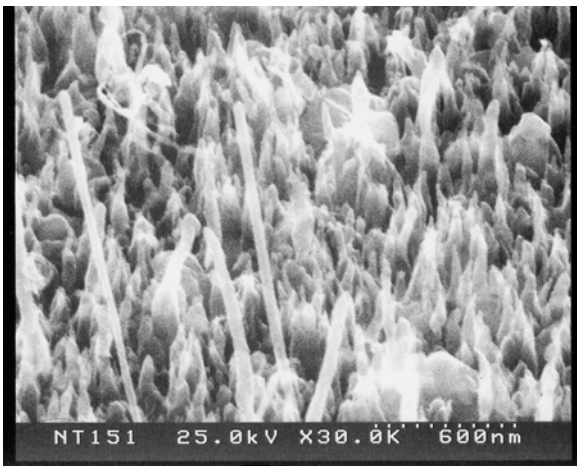
(b) 10 min

(d) 30 min

Fig. 39. SEM photographs of CNTs grown on stainless steel 304 at a negative bias of -300 V

for various periods; (a) 5 min, (b) 10 min, (c) 15 min, and (d) 30 min.

Figure 40 plots the I_D/I_G ratio derived from the Raman spectra obtained after various periods of growth of CNTs on stainless steel 304. The relative intensities of the two peaks depend on the type of graphitic material. As the ratio of the intensity of the disorder peak at 1335 cm^{-1} to that of the graphite carbon peak at 1590 cm^{-1} (I_D/I_G ratio) decreases, the degree of graphitization increases. Figure 40 shows that the I_D/I_G ratio decreases as the growth period increases. Restated, this figure shows that the crystallinity of the CNTs becomes better as the growth period increases. The SEM photographs show that the product on the samples becomes more uniform and coherent as time passes. The better crystallinity of the CNTs is believed to be attributable to the reduction in the amount of disorganized carbon in the samples.
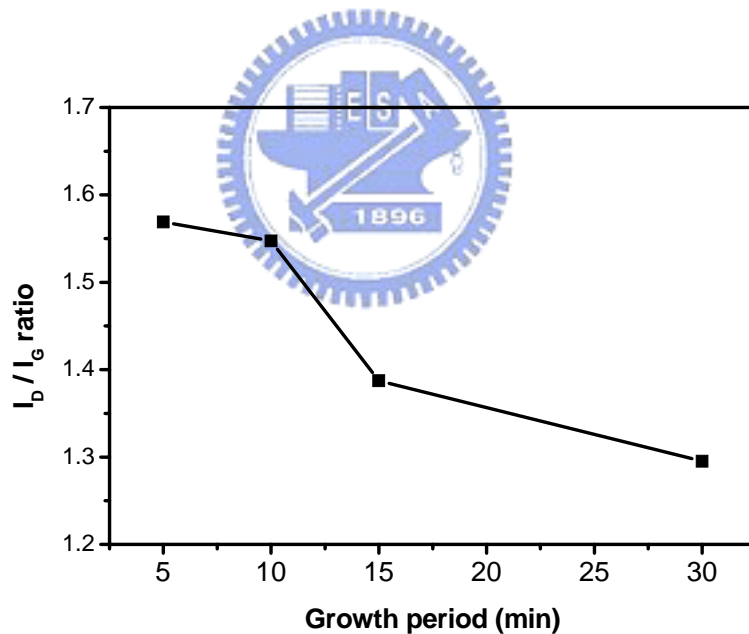

Fig. 40. I_D/I_G ratio derived from micro-Raman spectra of CNTs grown over various periods on stainless steel 304.

Figure 41 and 42 show TEM images of the product grown on the stainless steel 304 for 5 min. As shown in Fig. 41, the CNTs were analyzed by TEM to confirm that the tubes are multi-walled CNT. Besides, it suggests that the catalysts are on the top of the CNTs. Figure 42 reveals TEM images of the carbon related nano-structure grown on stainless steel 304 for 5 min. Therefore, it is found that CNTs and other carbon related nano-structure should coexist in this growth stage. It should be noted that temperature of substrate still increases during this short period.

Fig. 43-45 shows TEM images of the end section of three individual CNTs grown for 30 min. The CNTs were analyzed by TEM to confirm that they were truly CNTs, and not solid carbon fibers. A comparison of these images to those presented elsewhere [174] indicates that the tubes are multi-walled CNTs. These images also reveal that the CNTs have inner diameters of 10-20 nm, and outer diameters of 30-40 nm. A comparison of these images with the SEM photograph in Fig. 39(d) suggests that the catalyst is on the top of the CNTs. It is according the fact that the diameter of the CNTs' top seem to be smaller than the bottom.

A high concentration of hydrogen plasma and a high negative bias applied to the substrate were found to enable the randomly oriented carbon nanotubes to be easily removed by anisotropic etching. Such a mechanism can remove all carbon nanotubes that are not parallel to the hydrogen plasma attracted to the substrate under a negative dc bias [178]. Therefore, CNTs and other carbon related nano-structure that coexisted in the initial growth stage should be selectively removed by anisotropic etching. As the growth continued, random carbon related nano-structure materials are etched gradually, and aligned CNTs are final product. Besides, the reduction in the amount of disorganized carbon in the samples was found by micro-Raman spectra.
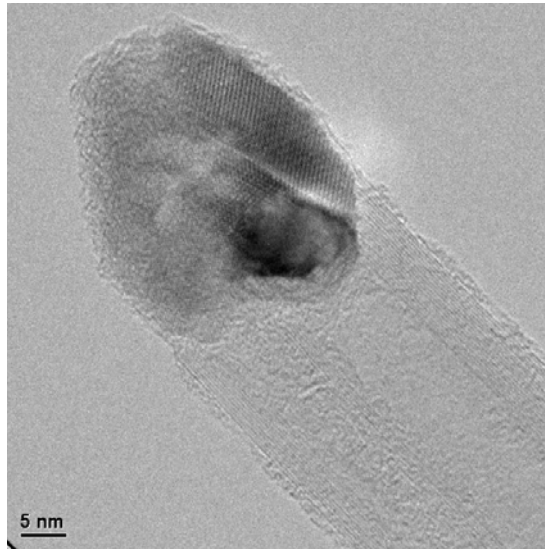
5 nm

Fig. 41. TEM image of the end section of CNTs grown on stainless steel 304 for 5 min.
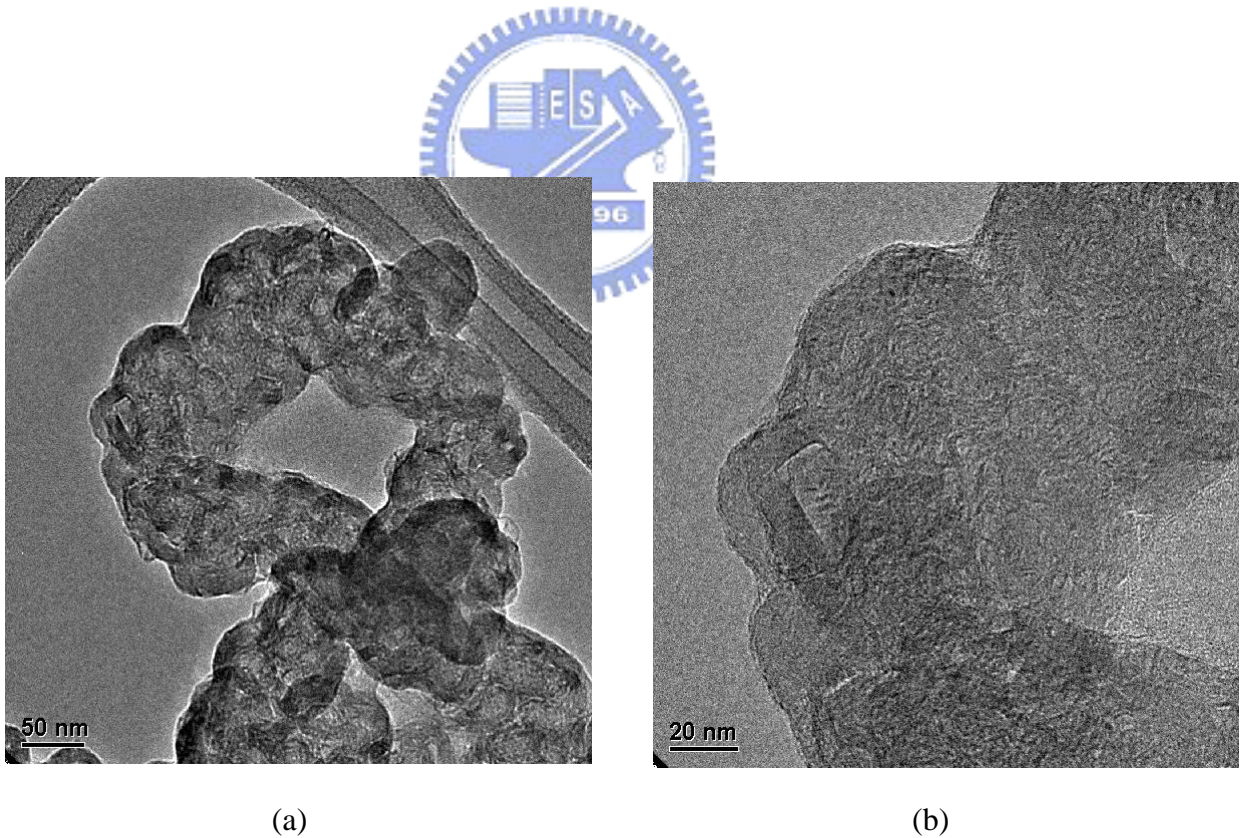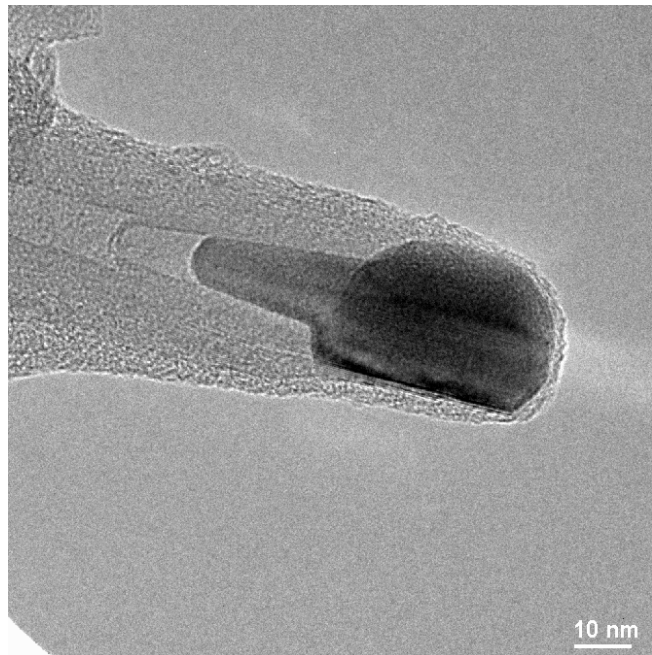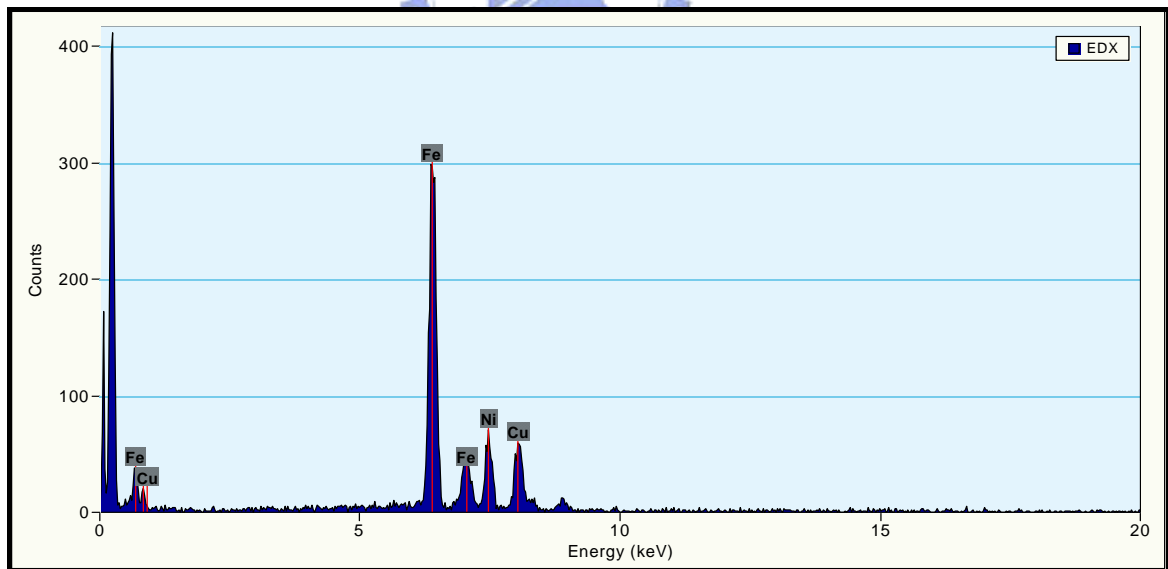

50 nm

(a)

20 nm

(b)

Fig. 42. TEM images of the carbon related nano-structure material grown on stainless steel 304 for 5 min; (a) scale bar is 50 nm, and (b) scale bar is 20 nm.
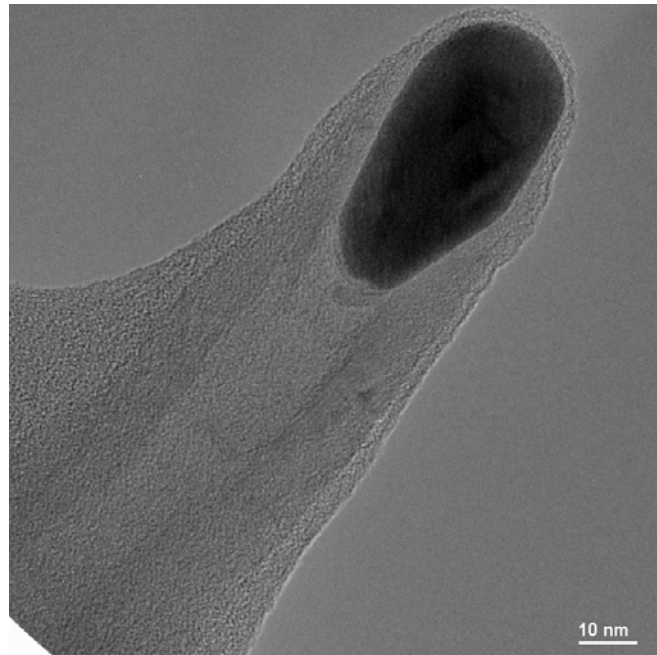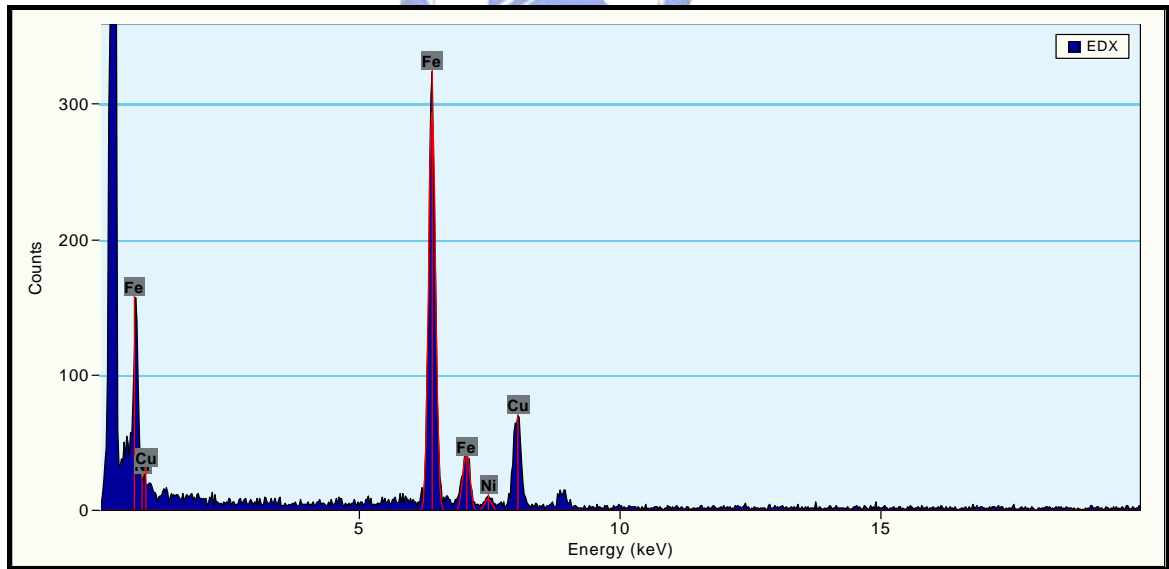
76

(a)

(b)

Fig. 43. (a) TEM image of the end section of individual CNTs grown on stainless steel 304

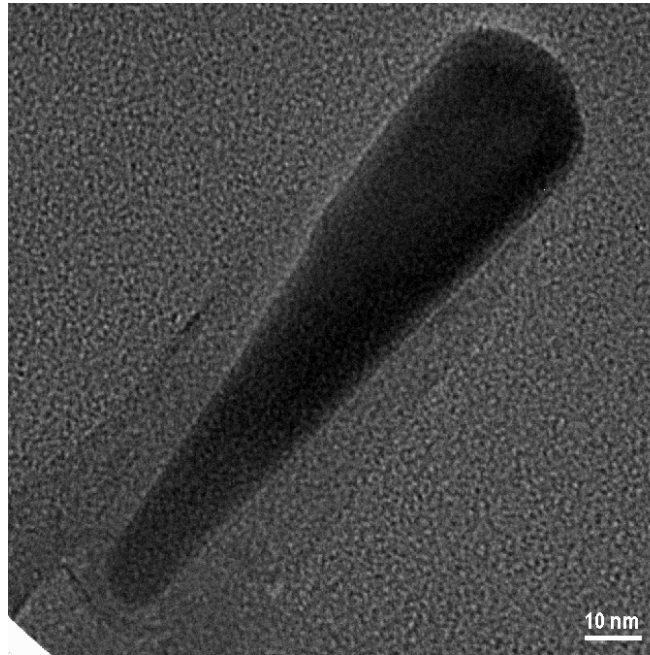for 30 min, and (b) EDX analysis of catalyst particle (Sample number 1).
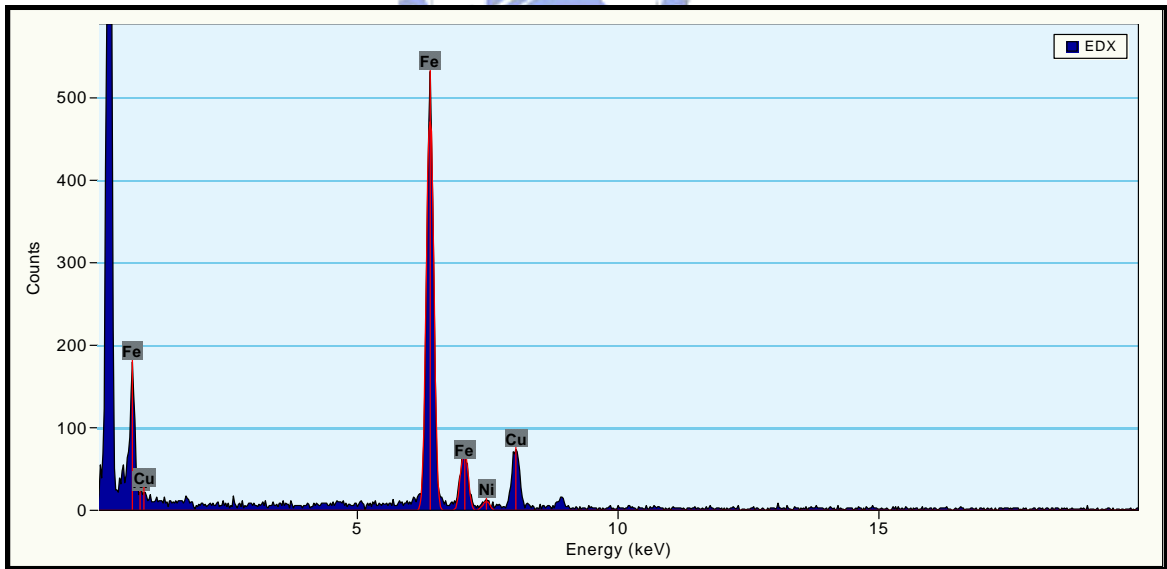
(a)

(b)

Fig. 44. (a) TEM image of the end section of individual CNTs grown on stainless steel 304

for 30 min, and (b) EDX analysis of catalyst particle (Sample number 2).
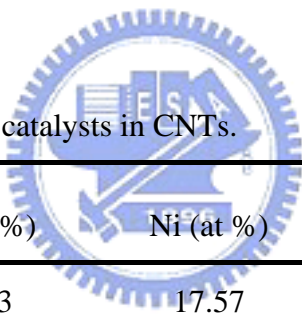
(a)

(b)

Fig. 45. (a) TEM image of the end section of individual CNTs grown on stainless steel 304

for 30 min, and (b) EDX analysis of catalyst particle (Sample number 3).

4.3.4 Catalytic Effect of Metal

Table 7 presents EDX analyses of metal catalysts in CNTs. Figures 43, 44 and 45 refer to samples 1, 2 and 3, respectively. In these ten samples, EDX signal of Cr is not observed. The top metal particles therefore include only Fe and Ni, but not Cr when the carbon nanotubes are grown on the 304 alloy substrate. According to the binary phase diagrams of carbon and metal [179], as shown in Fig. 46, the eutectic point of C-Cr alloy (1533 ℃) is higher than that of C-Fe (1153 ℃) and C-Ni (1326 ℃) alloys, which fact is one reason for the elimination of Cr from Fe-Ni-Cr alloy [28]. SEM at low magnification revealed that particles were present along the grain boundary of stainless steel 304. We therefore suggest that chromium carbide is precipitated in the grain boundary of stainless steel at an elevated temperature, in a process similar to that which occurs when stainless steel is heat-treated.

Table 7 EDX analyses of metal catalysts in CNTs.

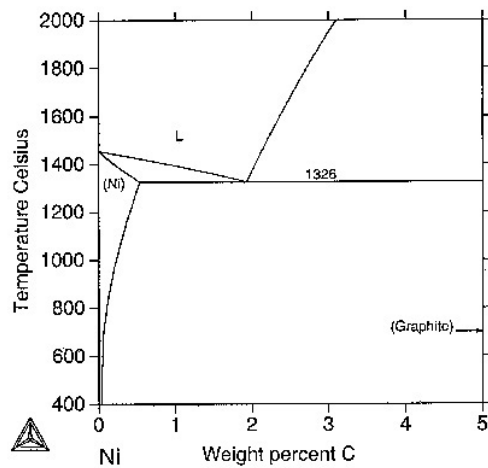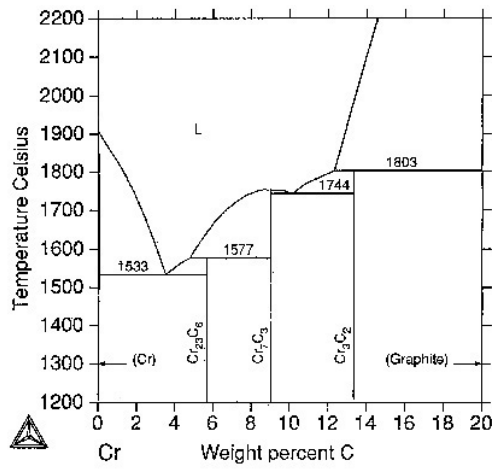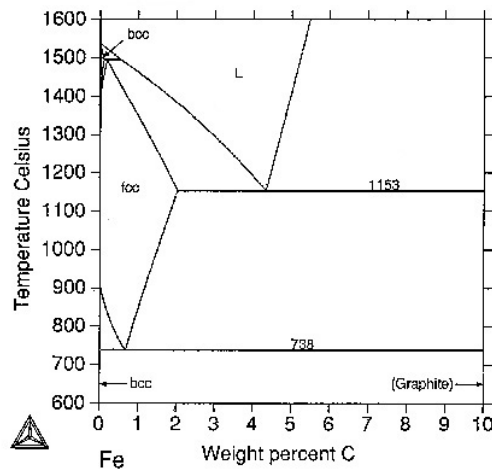| Sample No.	Fe (at %)	Ni (at %)	Fe (wt %)	Ni (wt %)
1	82.43	17.57	81.70	18.30
2	97.03	2.97	96.89	3.11
3	97.63	2.37	97.51	2.49
4	95.59	4.41	95.37	4.63
5	89.70	10.30	89.23	10.77
6	95.07	4.93	94.83	5.17
7	97.81	2.19	97.71	2.29
8	81.93	18.07	81.18	18.82
9	79.04	20.96	78.20	21.80
10	87.18	12.82	86.61	13.39

Fig. 46. Binary phase diagrams of C-Fe, C-Cr and C-Ni [179].

4.3.5 Field Emission Properties

The field emission properties of CNTs grown at a -300 V bias for 30 min are obtained using a diode structure. An anode, made of ITO glass, was separated by 500 μm from the tip of a cathode made of CNTs. The *I-V* properties were measured using an electrometer (Keithley 237) and analyzed using the Fowler-Nordheim (F–N) model. Figure 47 plots emission current against applied voltage, and also presents an F-N plot of this sample. The F–N plot is used to confirm the field emission characteristics. A linear relationship between ln (I/V^2) and 1000/V is obtained. The emission current at an applied voltage of 1000 V (2 V/μm) was 314 μA (140 μA/cm^2). The macroscopic turn-on field, which is the field needed to extract a current density of 10 μA/cm^2, was 700 V (1.4 V/μm).
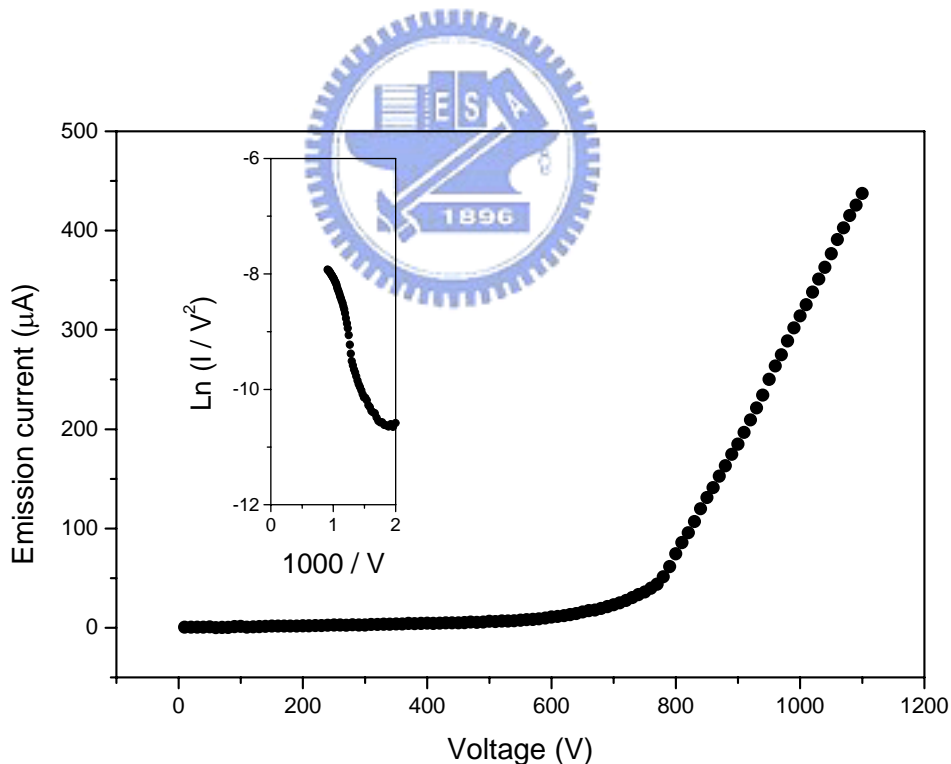

Fig. 47. Emission current against applied voltage, and F-N plot of CNTs grown on stainless steel 304 at -300 V bias for 30 min.